Carbohydrate Polymers 101 (2014) 741–751

Contents lists available at ScienceDirect

Carbohydrate Polymers

journal homepage: www.elsevier.com/locate/carbpol

One-pot synthesis of biocompatible superparamagnetic iron oxide nanoparticles/hydrogel based on salep: Characterization and drug delivery

Ghasem Rezanejade Bardajee*, Zari Hooshyar

Department of Chemistry, Payame Noor University, PO Box 19395-3697, Tehran, Iran

ARTICLE INFO

Article history:
Received 17 June 2013
Received in revised form 29 August 2013
Accepted 9 October 2013
Available online 16 October 2013

Keywords:
Magnetic iron oxide nanoparticles
Hydrogel
Salep
Drug delivery

ABSTRACT

This work describes synthesis of biocompatible magnetic iron oxide nanoparticles/hydrogel based on salep (MION–salep hydrogel) by a facile one-pot strategy. The prepared sample was characterized by techniques like scanning electron microscopy with energy dispersive X-ray analysis (SEM-EDAX), transmission electron microscopy (TEM), Fourier transform infrared spectroscopy (FT-IR), thermal gravimetric analysis (TGA), and vibrating sample magnetometer (VSM). The obtained MION had an 8 nm diameter with a narrow size distribution and was superparamagnetic with large saturation magnetization at room temperature. The most attractive feature of the obtained sample was its swelling properties under external magnetic field (EMF), different temperatures, and pHs. Moreover, MION–salep hydrogel showed ability to deferasirox release at pH = 7 with non-Fickian diffusion mechanism. An in vitro cytotoxicity study implied that the as-synthesized sample is nontoxic.

1. Introduction

Magnetic iron oxide nanoparticles (MION) have received much attention over the past decade because of their unique magnetic properties such as small size (Qin, Li, Hu, Shen, & Ye, 2009), limited toxicity (Figuerola, Corato, Manna, & Pellegrino, 2010), low cost of production (Goloverda, Jackson, Kidd, & Kolesnichenko, 2009), ease of separation and detection (Mahmoudi, Sant, Wang, Laurent, & Sen, 2011; Monson et al., 2013). They have been extensively used in various applications, for instance, nanoprobes for in vivo imaging (Krukemeyer, Krenn, Jakobs, & Wagner, 2012), contrast agents in magnetic resonance imaging (Andreas et al., 2012), immobilization of enzyme (Jain et al., 2009), magnetizable implants for targeted drug delivery (Vu-Quang et al., 2011; Likhitkar and Bajpai, 2012), stimuli-responsive systems (Figuerola et al., 2010), hyperthermia treatments (Xu et al., 2011), environmental analysis and magnetic separations (Parham, Zargar, & Rezazadeh, 2012; Parham, Zargar, & Shiralipour, 2012). However, the MION tend to form large aggregates owing to the strong magnetic dipole–dipole attractions among particles (Gordon et al., 2011; Jayapaul et al., 2011). To improve their stability and biocompatibility, the surface of MION have been modified with various surfactants (Jiang, Fu, Zhu, Tang, & Sheng, 2012), oxide (Easo & Mohanan, 2013) or polymeric compounds (Calmon et al., 2012; Cole, David, Wang, Galbán, Hill, et al., 2011; Lai, Yeh, & Chen, 2012; Schweiger, Pietzonka, Heverhagen, & Kissel, 2011; Vu-Quang et al., 2012). In fact, polymers with more than one group capable of binding to particle surfaces (multidentate ligands) provide mechanical and chemical stability to the MION. Furthermore, three-dimensional networks of cross-linked polymers which are called hydrogels enable the encapsulation of MION (Fuhrer, Athanassiou, Luechinger, & Stark, 2009; Hernández & Mijangos, 2009; Rubio-Retama et al., 2007; Yu, Hsieh, et al., 2013). It is expected that the combination of MION and hydrogels constitute a novel functional composite keeping both hydrogel and MION properties.

Hydrogels are hydrophilic polymeric materials that are able to retain the large amounts of water needed or biological fluids in their three-dimensional networks without being dissolved (Guo et al., 2013; Luo, Teng, Wang, & Wang, 2013; Paques, Linden, Rijn, & Sagis, 2013). The hydrophilicity of the network is due to the existence of chemical residues such as —OH, —COOH, —NH_2, —$CONH_2$, —SO_3H, and others that can be found within the polymer backbone or as lateral chains. Their soft, flexible nature, resemblance of natural living tissue and inherent biocompatibility have made hydrogels as suitable carrier for pharmaceutical applications such as oral drug delivery (Palmer et al., 2013; Perez-Moral & Gonzalez, 2013), wound dressing (Jovanović et al., 2013), tissue engineering (Gajendiran, Gopi, Elangovan, Murali, & Balasubramanian, 2013), and so on. In addition, hydrogels make a volume change with water filled in the cavity of networks or drained by the shrinkage of networks accompanying with the variation of the extra condition, such as pH

* Corresponding author. Tel.: +98 281 3336366; fax: +98 281 3344081.
E-mail addresses: grezanejad@ymail.com, rezanejad@pnu.ac.ir (G.R. Bardajee).

0144-8617/$ – see front matter © 2013 Elsevier Ltd. All rights reserved.
http://dx.doi.org/10.1016/j.carbpol.2013.10.028

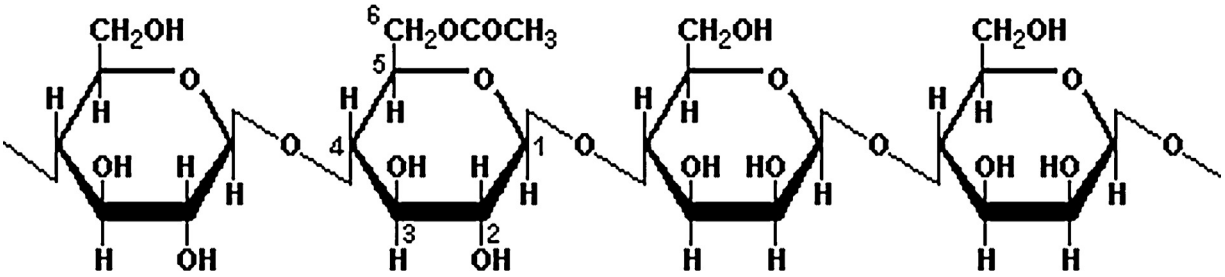

Fig. 1. A portion of the glucomannan repeating unit.

(Debrassi et al., 2011; Gui, Wan, Jin, Li, & Zhou, 2013; Yu, Wu, et al., 2013), light (Cursaru, Teodorescu, Boscornea, Stanescu, & Stoleriu, 2013; Pichayakorn & Boonme, 2013), temperature (Shirsath et al., 2013; Tang, Huang, Qian, & Benicewicz, 2013), and ionic strength (Matalanis & McClements, 2013). This stimuli-responsive property makes them having many potential applications, such as smart drug delivery systems, that release drugs by diffusion through their porous structure under specific stimulation.

Wide ranges of hydrophilic polymers have been examined to synthesize MION/hydrogels. Among them, polysaccharide-based hydrogels have received a great deal of attention because of their low cost (Chung et al., 2012), low toxicity (Shen et al., 2011), biocompatibility (Liang, Zhang, Jiang, & Li, 2007), biodegradability (Hernández & Mijangos, 2009), and nontoxicity (Dias, Hussain, Marcos, & Roque, 2011). Liang et al. have fabricated biocompatible polysaccharide-based hydrogels with stimuli-responsive properties by the copolymerization of maleilated carboxymethyl chitosan with N-isopropylacrylamide, and then embedding of MION into the porous hydrogel networks (Hezaveh & Muhamad, 2012). Their resultant hybrid hydrogels could retain the pH- and temperature-responsive characteristics of their hydrogel precursors. Hernández et al. reported in situ oxidation of iron cations coordinated to semi-interpenetrating polymer network based on alginate and poly(N-isopropylacrylamide) with response to temperature and magnetic fields (Easo & Mohanan, 2013). Many other works have also been reported in the case of preparation of MION/hydrogels based on agarose (Dias et al., 2011), carrageenan (Hezaveh & Muhamad, 2012), dextran (Brunsen, Utech, Maskos, Knoll, & Jonas, 2012), heparin (Lee et al., 2012), gum Arabic (Roque, Bicho, Batalha, Cardoso, & Hussain, 2009), alginate (Nishioa et al., 2004), salep (Saeidian et al., 2009) and starch (Cole, David, Wang, Galbán, & Yang, 2011). In all the above prepared MION/hydrogels, two main approaches have been applied. In the first method, hydrogel and MION have been prepared separately and then were mixed together. By this method, the structure and component of the hydrogels can be controlled seperately but the obtained MION are not stable and it may leach from the polymer matrix without strong anchoring. In the second method, the preformed MION have been initially incorporated into the polymer by mixing and then MION/hydrogels have been prepared by in situ cross-linking. The most drawback of this method is the easily aggregation of preformed MION in the hydrogel network which may be harmful for biological application. Moreover, in the mentioned methods, various crosslinkers such as ammonium persulfate, glutaraldehyde, bis(sulfosuccinimidyl)suberate, D,L-glyceraldehyde, and genipin have been used to crosslink polysaccharide solutions. Although the treatment by chemical reagents is effective in yielding a high degree of crosslinking, the chemical residuals are highly cytotoxic, which restrict their potential applications in the biomedical field (Kuckling, Harmon, & Frank, 2002; Shen, Duan, & Frey, 2007). In addition, preparation of sited MION/hydrogels required number of processing steps and time.

Recently, Zhou, He, and Zhang (2012) successfully synthesized magnetic poly(vinyl alcohol) (mPVA) gel beads by dropwise addition of mixed aqueous solution of iron salts and PVA solution into alkaline (e.g., ammonia, NaOH, and KOH) solution. This synthetic process is facile and fast because of the MION and gels were achieved in the same reactor by one step process. Therefore, this is an effective approach to scalable synthesis of MION/hydrogels without using any chemical crosslinking agent. Also, simultaneous in situ formation of MION and crosslinked PVA chains leads to the stable and uniform dispersion of MIONs in PVA matrix. However, to the best of our knowledge, preparation of MION/hydrogels based on polysaccharides has not been reported by aforementioned method.

Salep as a polysaccharide backbone has a several merits, including non-toxic (Pourjavadi, Hosseini, & Fakoorpoor, 2013; Wang et al., 2008), low cost (Bardajee, Hooshyar, & Jafarpour, 2013; Li et al., 2011), abundant in nature (Ktistis & Georgakopoulos, 1991), and gelling properties (Pourjavadi, Doulabi, Soleyman, Sharif, & Eghtesadi, 2012) which are explored for a variety of life science and drug delivery applications (Bardajee, Hooshyar, & Rezanezhad, 2012; Ha et al., 2011). Salep as a source of glucomannan is obtained from dried tubers of certain natural terrestrial orchids. It has attracted considerable attention because of its nutritive and demulcent properties (Gao, Guo, & Nishinari, 2008; Kaya & Tekin, 2001; Ktistis & Georgakopoulos, 1991). The glucomannan of salep (Orchidaceae) has a linear chain of heteropolysaccharide with 1:3.8 ratios of glucose and mannose, in which hexopyranoses are connected together by $1 \rightarrow 4$ linkages. Fig. 1 depicts the chemical structure of glucomannan. Glucomannans can help to normalize blood sugar, reduce stress on the pancreas, and discourage blood sugar abnormalities such as hypoglycemia (Hozumi et al., 1995). It can also operate as a preventative of chronic disease (Vuksan et al., 1999), a weight control agent (Ha et al., 2013; Reffo, Ghirardi, & Forattani, 1990; Walsh, Yaghoubian, & Behforooz, 1984) and is considered to be a useful advance in treatment of chronic constipation in adult patients (Marzio, Bianco, Donne, Pieramico, & Cuccurullo, 1989). The compositional components and rheological behavior as a function of concentration and temperature for salep in Iran were investigated (Farhoosh & Riazi, 2007). In addition to glucomannan, the results showed that salep also contains starch (2.7%), nitrogenous substance (5%), moisture (12%) and ash (2.4%) (Farhoosh & Riazi, 2007; Kaya & Tekin, 2001; Wang, Liao, Huang, & Cheng, 2011).

In this study, we attempted to prepare MION–salep hydrogels in a facile one-pot strategy without using any chemical crosslinkring or usual initiators. Physicochemical properties of the MION–salep hydrogel such as swelling behavior, morphology, and thermal stability were investigated. Furthermore, their biological properties and cytotoxicity were evaluated. On account of MION–salep hydrogel properties and a facile fabrication procedure, the MION–salep hydrogel are expected to have marvelous prospects as scaffolds for biological field.

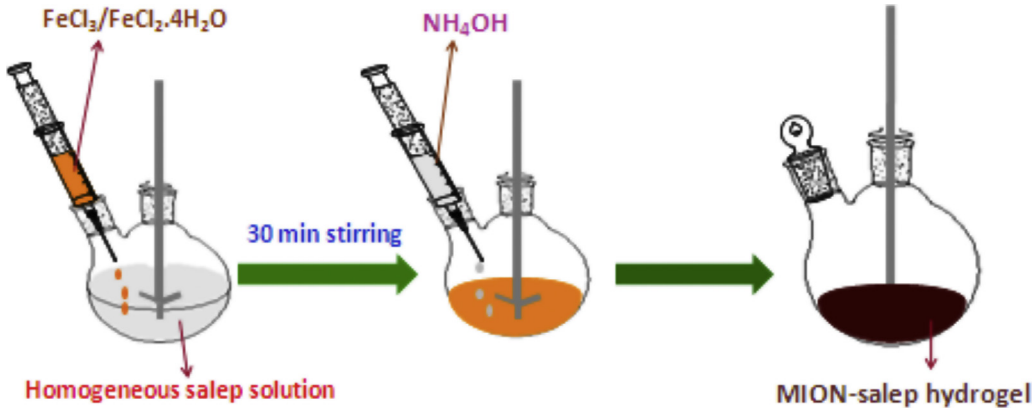

Scheme 1. Schematic illustration of synthetic procedure for the MION–salep hydrogel.

2. Experimental

2.1. Chemicals and reagents

Salep ($M_n = 1.17 \times 10^6$ g/mol, $M_w = 1.64 \times 10^6$ g/mol (high M_w), PDI = 1.39, eluent = water, flow rate = 1 mL/min, acquisition interval = 0.43 s from GPC results) was purchased from a supplier in Kordestan, Iran. Ammonium hydroxide (NH_4OH, from Scharlau, 25% (v/v)), iron (II) chloride tetrahydrate ($FeCl_2{\cdot}4H_2O$, from Sigma–Aldrich) and anhydrous iron (III) chloride ($FeCl_3$, from Sigma–Aldrich) were analytical grades and used without further purification. Deferasirox was received from Osveh pharmaceutical Co., Tehran, Iran as a gift. Gram-negative *Escherichia coli* (*E. coli*) and gram-positive *staphylococcus aureus* (*S. aureus*) bacteria were prepared from NIGEB Bacterial Bank (Tehran, Iran). Phosphate buffered saline (PBS), trypsin, dimethyl sulphur oxide (DMSO), Luria Bertani (LB) agar powder, and MTT formazan powder were purchased from Sigma–Aldrich. Double distilled water (DDW) was used throughout the experiments.

2.2. Syntheses of MION–salep hydrogel

The procedure for the synthesis of the MION–salep hydrogel was followed as Scheme 1. Typically, a homogeneous solution of salep (1.00 g salep in 40.00 mL DDW) was prepared in a 2-neck reactor equipped with a mechanical stirrer (600 rpm) which was placed in a thermostated water bath preset at 80 °C. After cooling solution, variety of $FeCl_3/FeCl_2{\cdot}4H_2O$ concentrations (0.37/0.1, 0.74/0.2, 1.1/0.3, 1.5/0.4, 1.85/0.5, and 2.23/0.6 mmol) were mixed in 20 mL of DDW and added drop wise to homogeneous solution of salep at room temperature with vigorous stirring. After 30 min stirring, by adding 20.00 mL of NH_4OH, the color of solution was changed from yellowish to black. To purify the hydrogel nanocomposite (removing the uncrosslinked salep, monomer and so on), the product was remained into 100.00 mL of ethanol for 2 h and then chopped to small pieces for further drying. In a continuation, it was allowed to completely swell for overnight in plenty of DDW (400.00 mL) and then dewatered in ethanol (200.00 mL, 2 h) again. The dewatered gel particles were filtered and dried in oven (at 50 °C) for 24 h. After grinding, the obtained powder was stored in the absence of moisture, heat, and light for further experiments.

2.3. Degree of swelling

Swelling capacity of the MION–salep hydrogel was determined gravimetrically. In this way, 0.50 g of MION–salep hydrogel placed in a tea bag (i.e. a 100.00 mesh nylon screen) and immersed entirely in 100.00 mL of DDW or desired pH phosphate buffer solutions (pHs = 2–10) for definite times. In order to remove the excess solution, the tea bag was hung up for 5 min. The degree of swelling was determined from equation:

$$\text{Swelling (g/g)} = \frac{\text{Weight of swollen gel}}{\text{Weight of dried gel}} - 1 \quad (1)$$

2.4. Drug loading and releasing studies

Drug loading can be performed by one of the following ways: (1) adding of the drug into the hydrogel during the preparation of the hydrogel, (2) allowing the hydrogel to swell in the drug solution until reach to equilibrium swelling (Ali & AlArifi, 2009; Gupta & Shivakumar, 2010). In this work, the later method was adopted to drug loading because of the problems in purification of the drug loading in the former method.

Typically, deferasirox was loaded into MION–salep hydrogel by dispersing 0.05 g of MION–salep hydrogel in 5.0 mL deferasirox solution with various concentrations (0.033, 0.038, 0.043, and 0.048 mg/mL) which was shaken in a rotary shaker (200 rpm) at 37 °C. For drug loading tracing, the amount of loaded drug was determined at favored times by UV spectroscopy (λ_{max}) using a calibration curve constructed from a series of drug solutions with known concentrations. After that the loaded MION–salep hydrogel was dried in oven at 50 °C. For drug releasing study, the dried gel was dispersed in 20.0 mL phosphate buffer (pH = 2 and 7) in a rotary shaker (200 rpm) at 37 °C. At specific intervals, 1.00 mL filtered samples were withdrawn to measure the optical density of drug release. Finally, the amount of drug releasing was calculated at 297 nm by UV–vis spectrophotometer.

2.5. Cytotoxicity evaluation of MION–salep hydrogel

For cytotoxicity assays, human bladder epithelial cell line HTB 5637 (ATCC HTB-9) was grown in Dulbecco's Modified Eagle's Medium (DMEM) (Invitrogen) supplemented with 10% fetal bovine serum (HyClone, Logan, UT). The cells then were trypsinized, counted and in each well of 96 ELISA plate, 5000 cells were seeded and different concentration of MION–salep hydrogel were added to the cells. After 24 h, the MTT assay was done. The culture of control cells was carried out under similar conditions in a culture medium without added MION–salep hydrogel. The cells were observed by an inverted microscope, in order to assess their morphology and to check their overall health after exposure to MION–salep hydrogel.

2.6. Instrumentation

Fourier transforms infrared (FT-IR) spectroscopy measurements were carried out at room temperature on a Jasco 4200 FT-IR

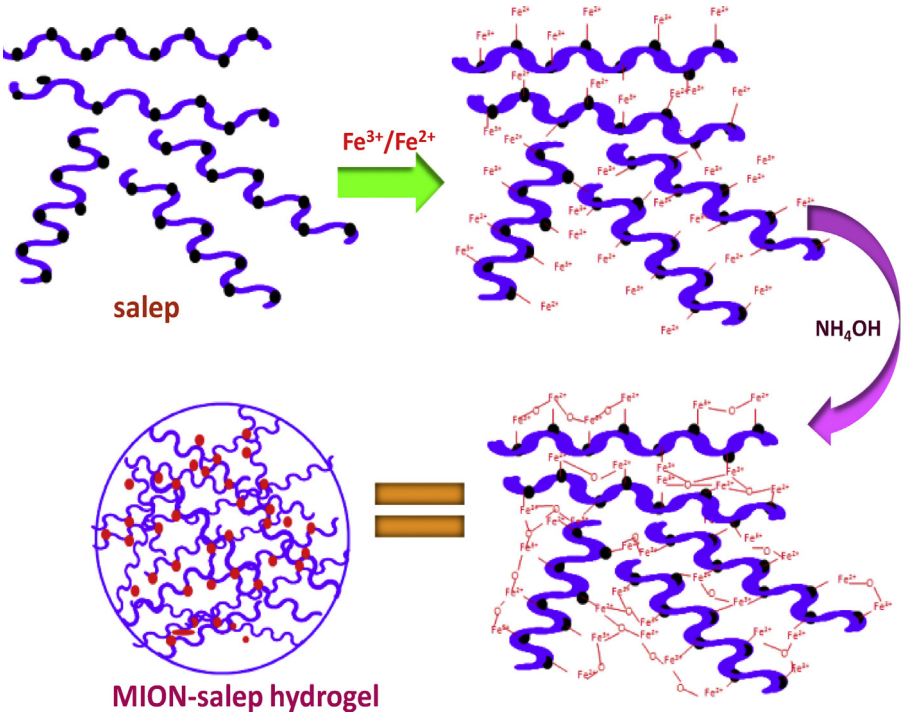

Scheme 2. Proposed mechanism for preparation of MION–salep hydrogel.

spectrophotometer. TGA was performed by heating the samples under N_2 flow at a rate of 25 mL/min using a TA instrument 2050 thermo-gravimetric analyzer with a heating rate of 20 °C/min. Scanning electron microscopy (SEM) with energy dispersive X-ray analysis (EDAX) (Hitachi S-5200 SEM) and transmission electron microscopy (TEM; Hitachi H-700 CTEM) were used to examine the morphology and dimensions of hydrogel nanocomposites. UV–vis absorption spectroscopy measurements were performed on a Shimadzu UV–visible 1650 PC spectrophotometer using 1 cm path length quartz cuvettes. Magnetic studies at room temperature were carried out using vibrating sample magnetometer (VSM) (Model 880 from ADE technologies, USA). Carl Zeiss inverted microscope (Germany) was used for cell culture procedure.

3. Results and discussion

3.1. Synthesis and mechanism aspects

Scheme 2 shows the mechanism of in site synthesis of MIONs which was carried out in a salep solution. Salep was employed as a splitting medium for MION clusters and a stabilizer for fabricated MIONs. Soluble salep, which is mainly containing of glucomannan, is a straight-chain polymer formed by α-(1–4) linkages between β-glucose units, with a small amount of branching. Its hydroxyl groups are the best chelating sites to form complexation with Fe^{3+} and Fe^{2+} ions. This step which is called nucleation can be followed by growth step with adding NH_4OH aqueous solution. In this step, growth of MION was controlled by straight-chain polymer. These formed MION in the polymeric chain acted as crosslinking agent and formed three network structures. Therefore, the second step was highly dependent on the amount of salep in the solution. In fact at the higher concentration of polymer, the macromolecules came close and that ease to form cross linking. This suggested mechanism is consistent with similar studies on the preparation of nanoparticles in other solutions (Gordon et al., 2011).

3.2. Swelling study

The MION–salep hydrogels with different concentrations of $FeCl_3/FeCl_2$ were allowed to swell in DDW at room temperature (Fig. 2a). The results indicated that the swelling was increased with rising $FeCl_3/FeCl_2$ concentration up to 1.5/0.4 mmol and then it was decreased. The first increase in swelling capacity of MION–salep hydrogel was probably due to the higher cross-linking of polymeric chains. However, more increasing of $FeCl_3/FeCl_2$ concentration formed a tight and dense structure which hindering the diffusion of water through the hydrogel and leads to a decrease in water absorbency (Zhou et al., 2012). In the remainder of this manuscript, the MION–salep hydrogel content of 1.5/0.4 mmol $FeCl_3/FeCl_2$ was chosen as the optimum sample and used for further investigations.

In a continuation, it was found that the MION–salep hydrogel had magnetic responsibility. When a magnet was put near to the suspension, the MION–salep hydrogel were moved toward the magnet direction quickly, demonstrating that the MION–salep hydrogel possess magnetic properties (Fig. 2b). It indicated that this MION–salep hydrogel can interact with an external magnetic field (EMF) and be positioned to a specific place. To evaluate more on the magnetic sensitivity of MION–salep hydrogel, swelling experiments were carried out in the presence and absence of EMF. Fig. 2b illustrates the effect of EMF on the swelling kinetic of MION–salep hydrogel in DDW at room temperature. From both curves, at the starting times (below 90 min), the increase in the weight of the swollen MION–salep hydrogel was directly related to the time of swelling. The swelling behavior observed was associated with the absorption mechanism, which in turn, was determined by the diffusion process. It can be seen from Fig. 2b that swelling increased sharply upon prolongation of the swelling time up to about 90 min and then leveled off thereafter. Comparing two curves shows that the swelling capacity of MION–salep hydrogel is lower in the presence of EMF. It is probably due to attract of MION adjacent neighbors under EMF and so reduce distance between the MION as a result of attraction force induced by a given EMF. This phenomena cause to

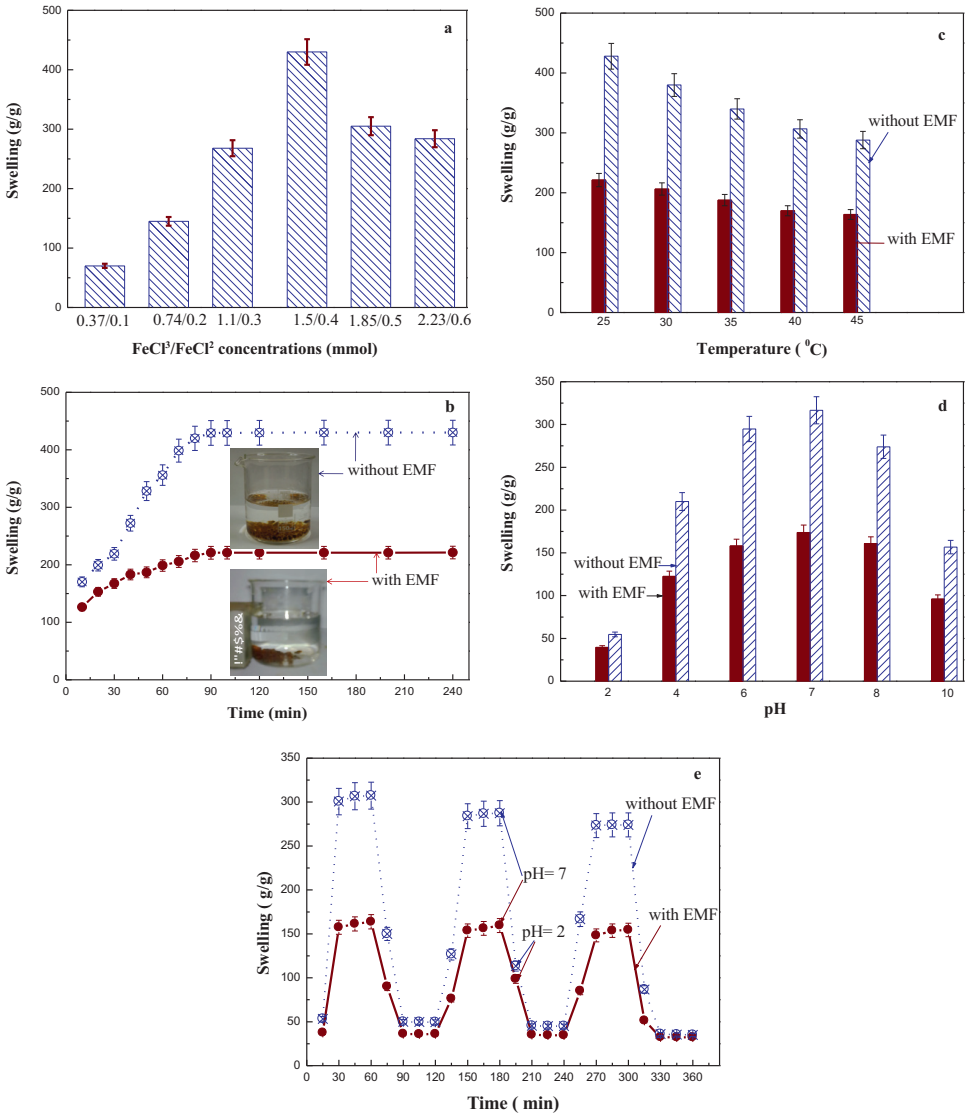

Fig. 2. (a) Effect of $FeCl_3/FeCl_2$ concentration (after 90 min at room temperature), (b) effect of EMF (at room temperature), (c) effect of temperature (in DDW after 90 min), (d) effect of pH on the swelling behavior of MION–salep hydrogel at 37 °C after 90 min, and (e) On–off switching behavior of the MION–salep hydrogel in phosphate buffer solutions with pH = 2 and 7 at 37 °C.

produce close-packed shells of MION which can block the diffusion of water into MION–salep hydrogel. These results were in accordance with those of the reports published by Liu, Hu, Liu, Liu, and Chen (2006).

The dependence of the MION–salep hydrogel swelling as a function of temperature over the range from 25 to 45 °C is shown in Fig. 2c. The swelling of MION–salep hydrogel is higher at low temperature due to the fact that hydrogen bonds between water molecules and hydrophilic groups lead to the good solubility of the MION–salep hydrogel at low temperatures. As the temperature increased up to 45 °C, the swelling of the MION–salep hydrogel decreased slowly which is due to the overwhelming of the hydrophobic groups on the hydrogen bonds, and phase separation occurs. In the other word polymeric chains of salep are expanded and uncrosslinked in the hydrogel systems, and tend to move alone (Khan, El-Toni, & Alhoshan, 2012). To more investigation, this experiment was also repeated in the presence of EMF. It also clears from Fig. 2c that same behavior with lower rate of swelling of MION–salep hydrogel is occurred in the presence of EMF. It seems that presence of EMF slightly prevents the phase separation of MION–salep hydrogel in high temperature.

Fig. 2d shows the effect of pH on the swelling behavior of MION–salep hydrogel in 100 mL of buffered solutions with pH = 2, 4, 6, 8 and 10 at 37 °C. As one can see in Fig. 2d, the swelling was much higher at the pH 7 comparing with the other pHs. The upper swelling at pH 7 can be attributed to the high repulsion between hydroxyl groups in the hydrogel networks in this medium. In higher acidic or basic solutions (pH = 2, 4 and 10), ionic strength of the medium is increased and the repulsion between aforementioned groups shielded by the counter ions from solution and results in lower absorbency. In addition, the pronounced acidic or basic media can catalyzed the hydrogen bond formation which mainly occurs between hydroxyl groups of polymer networks. This leads to lower degree of swelling at the supposed pHs (Bardajee et al., 2012). More experiments were carried out to study the effect of EMF on the swelling behavior of MION–salep hydrogel at different pHs. As shown in Fig. 2d, the same behavior with lower swelling in the presence of EMF was observed, which can be explained as above mentioned.

In order to consider the pH sensitivity of MION–salep hydrogel for potential use in site specific delivery of drugs to specific regions, we investigated their swelling reversibility at pH 2.0 and 7.0 in the

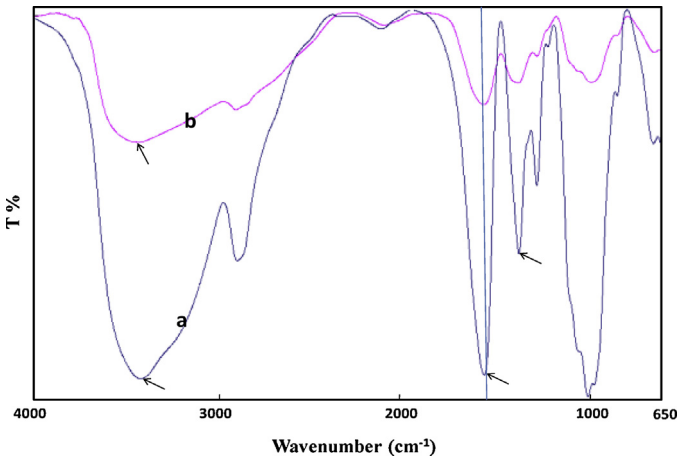

Fig. 3. FT-IR spectra of (a) salep, and (b) MION–salep hydrogel.

presence and absence of EMF. According to the presented results in Fig. 2e, MION–salep hydrogel showed good swelling–deswelling behavior which makes it as a suitable candidate for controlled drug delivery systems..

3.3. Spectral characterization

FT-IR spectroscopy was carried out to provide evidences that the MION–salep hydrogel were made up of salep and MION. In the spectrum of salep (Fig. 3a), the broad band at 3265 cm^{-1} is due to stretching vibration modes of hydroxyl functional groups. Two bands at 2930 and 1690 cm^{-1} are assigned to C—H band and C=O (ester moiety) stretching modes respectively. The bands at 1158, 1081, and 1014 cm^{-1} can be attributed to a C—O band vibrational stretching of salep. In the spectrum of MION–salep hydrogel (Fig. 3b), the bands are very close to the spectrum of salep. Also, considerable displacement occurred in the C=O band from 1690 cm^{-1} to the higher wave number side of 1720 cm^{-1}. This displacement of peaks occurred due to the electrostatic interaction between the C=O band and MION. The band at 569 cm^{-1} is characteristic adsorption of iron oxide due to the stretching vibrations of Fe—O, which is beyond the capacity of our facilities.

TGA was performed on salep and MION–salep hydrogel to determine the amount of formed MION in the MION–salep hydrogel. Fig. 4 shows the TGA/DTG/DTA of salep and MION–salep hydrogel. In detail, the salep has followed three endothermic decomposition steps and 82% degradation of the salep chains occurred below

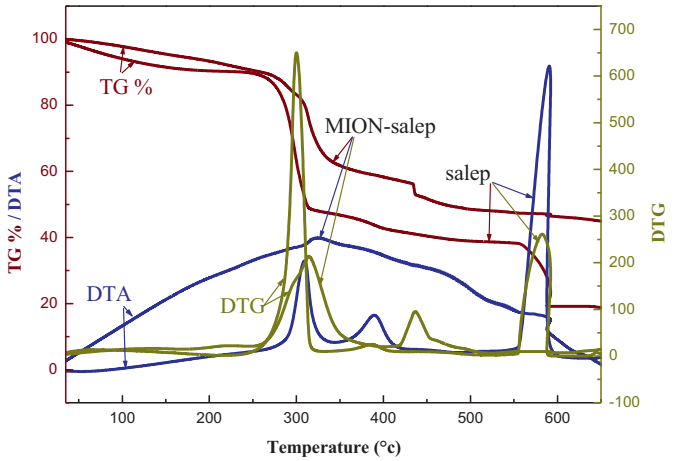

Fig. 4. TGA/DTG/DTA of salep and MION–salep hydrogel.

590 °C, as evidenced by its DTG curve. However, it is noted as three endothermic degradation steps and only a 48% weight loss below 590 °C in the case of MION–salep hydrogel. The weight loss or difference in decomposition between the salep and MION–salep hydrogel represents the amount of MION in the MION–salep hydrogel (Bardajee et al., 2012). In this particular sample, it is noted that there is a 34 wt% of MION content in the MION–salep hydrogel.

SEM analysis was performed to identify the morphology of MION–salep hydrogel. Fig. 5a clearly indicates the formations of many close-pores with uniformly distributed in MION–salep hydrogel structure. These pores are mainly responsible for swelling of MION–salep hydrogel (Gupta & Shivakumar, 2010). The MION were not obviously observed with SEM because of the large scale bar. Nevertheless, EDX mapping of iron showed that the MION was evenly distributed throughout the MION–salep hydrogel (Fig. 5b). To obtain more information about the size of the MION, TEM was used. Fig. 5c depicts the MION formed inside the MION–salep hydrogel are spherical, highly dispersed, and low nanometer in size. The related histogram exhibits the narrow distribution of particles with average particle size of 8 nm (Fig. 5d).

The superparamagnetic nature of the MION–salep hydrogel was determined by VSM at room temperature (Fig. 5e). The magnetic measurement studies showed that the MION–salep hydrogel exhibited superparamagnetic behavior, demonstrated by the symmetrical sigmoidal shape of the magnetization curves exhibiting no hysteresis (Reddy et al., 2011). These results suggest that the hydrogel matrix acts as effective stabilizer and prevents agglomeration phenomena during MION synthesis, which could have led to the formation of larger particles resulting in deviation from superparamagnetism.

3.4. Drug release

For a certain drug delivery system, the in vitro release behavior is a very good indication of the in vivo pharmacokinetics and biodistribution of the drug after its administration. To this aim, deferasirox was used as a model drug for loading and releasing experiments in the present study. Its structure (Fig. 6) show that it is a tridentate chelator which can coordinate to Fe atoms (Angelucci et al., 2000; Brittenham et al., 1982; Brittenham, Allen, Farrell, & Harris, 1989). Furthermore, the drug can be absorbed on the hydrogel networks by hydrogen bonding between the —OH and —COOH groups of the drug and —OH groups of salep. It was loaded into MION–salep hydrogel by swelling of preweighted MION–salep hydrogel (0.05 g) into the drug solution (5 mL) with different concentrations (0.033 (sample A), 0.038 (sample B), 0.043 (sample C), and 0.048 (sample D) mg/mL). The percentage of loaded deferasirox into MION–salep hydrogel was determined to be 86, 91, 95, and 97% for the samples A, B, C and D, respectively. These loaded hydrogels (A–D) were used to investigate the deferasirox release behavior in pH = 7 phosphate buffer. The amount of deferasirox release was measured by UV–vis spectroscopy. The obtained spectra are shown in Fig. 7. As shown in Fig. 7, there are no changes in the maximum absorption peaks of drug before and after releasing by hydrogels. It confirms the lack of chemical interaction between deferasirox and MION–salep hydrogel during loading and releasing experiments. To more investigation, the presence of iron in solution of deferasirox releases was also analyzed by atomic absorption spectrophotometer. The results showed that there is no iron in the sample solutions which confirmed that the MION did not leach from the hydrogel matrix during loading and releasing experiments.

Fig. 8a shows the deferasirox release profiles from the loaded hydrogels (samples A–D) with different concentrations of drug at pH = 7. To obtain a more quantitative understands of the kinetics of

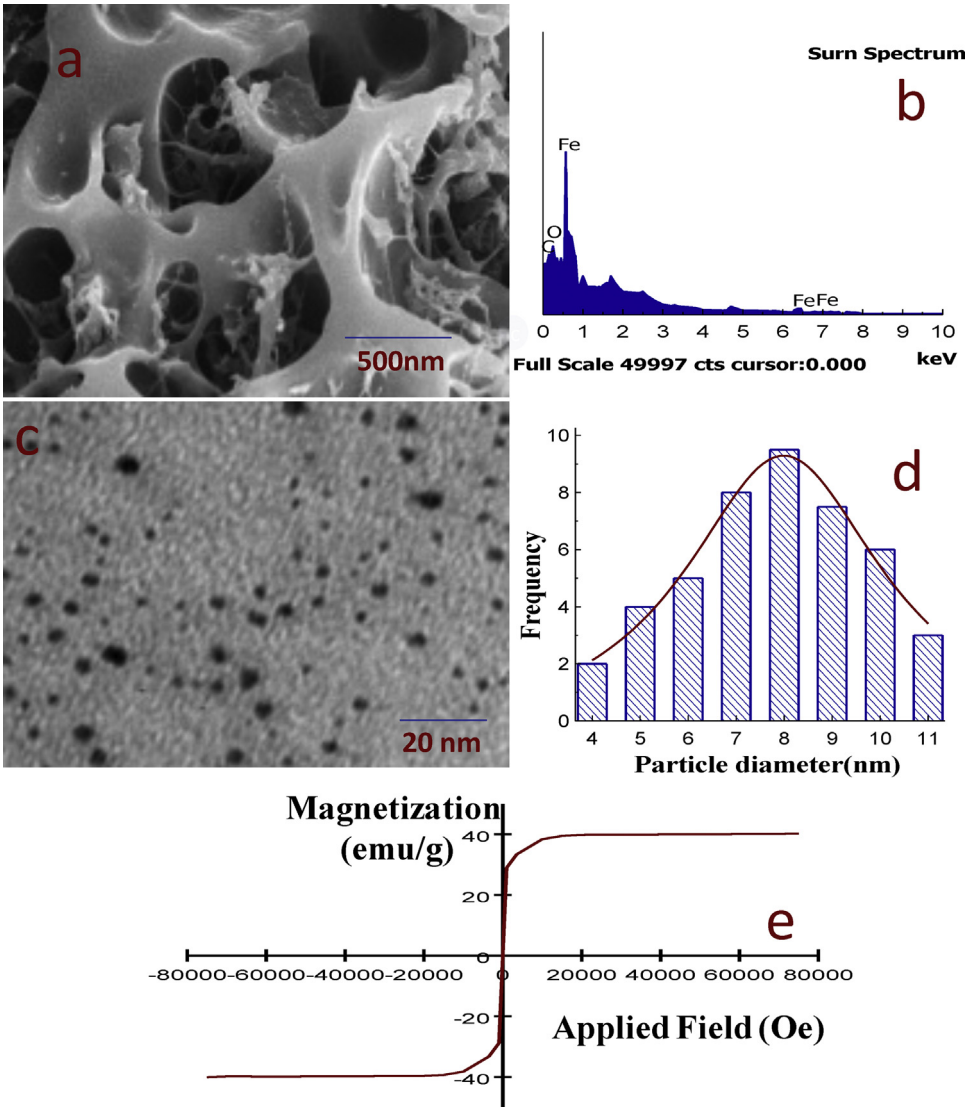

Fig. 5. (a) SEM, (b) EDAX, (c) TEM, (d) related histogram, and (e) VSM of MION–salep hydrogel.

the release, the release results were also analyzed using a power law type semiempirical equation (Debrassi et al., 2011):

$$\log\left(\frac{M_t}{M_\infty}\right) = \log k + n \log t \quad (3)$$

where (M_t/M_∞) = fractional solute release; M_t = mass of solute released at time "t"; M_∞ = mass of solute released at equilibrium; t = time; k = rate constant characteristic of the system and n = transport exponent indicating the release mechanism. The values of k and n are found by fitting the data to the above expression. For cylindrical shaped matrices, n was found to be around 0.45 implying that the diffusion is the controlling mechanism for drug release which is simply called Fickian type of diffusion. However, for $0.45 < n < 0.89$ an anomalous diffusion behavior is followed that is called non-Fickian type of diffusion and finally for $n > 0.89$, drug release shows a Case II (relaxational) transport which indicate a mechanism controlled by polymer relaxation and erosion, involving a relaxing boundary (dry glassy/hydrated rubbery polymer interface) moving into the matrix at an increasing rate.

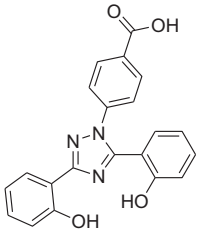

Fig. 6. Deferasirox chemical structure.

Fig. 8b shows $\log(M_t/M_\infty)$ vs. $\log t$ curves for deferasirox release from the above loaded hydrogels (samples A–D). Good linearity is shown, indicating that this equation is applicable to the present systems. By this plot, the release exponents of n, rate constant of $\log k$ and the correlation coefficient R^2 from the above loaded hydrogels were obtained and they are listed in Table 1. These data confirmed

Table 1
Release exponent (n), rate constant ($\log k$), and correlation coefficient (R^2) for deferasirox on its release profiles from loaded hydrogels (samples A–D; 0.05 g) at pH = 7 phosphate buffer.

Loaded hydrogels	Log k	n	R^2
A	0.658	0.350	0.990
B	−1.20	0.480	0.971
C	−0.540	0.316	0.983
D	−0.486	0.306	0.982

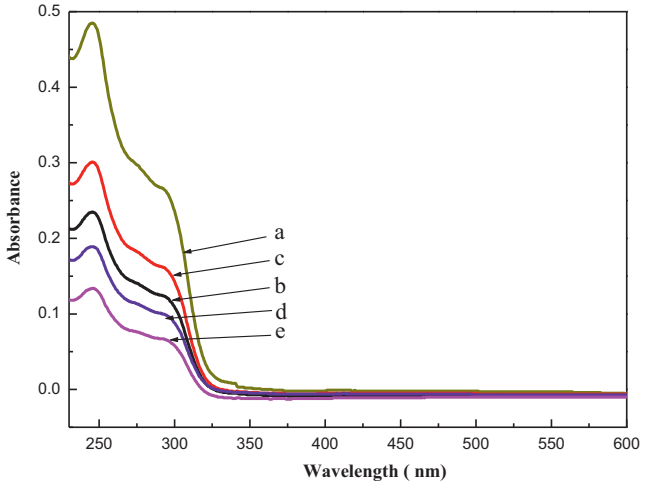

Fig. 7. Comparison of UV–vis spectra of (a) initial deferasirox, and deferasirox release from (b) sample A, (c) sample B, (d) sample C, and (e) sample D (loaded onto 0.05 g MION–salep hydrogels).

that the releases of deferasirox follow diffusion kinetics for hydrogel samples A, C, and D, and both diffusion and polymer relaxation kinetics for sample A.

The controlled release of deferasirox from the MION–salep hydrogel was also studied at pH = 2 for 6 h followed by at pH = 7 for 8 h for sample B, as shown in Fig. 9a. Result revealed that the in vitro drug release of deferasirox at pH 2 for first 6 h was very slow

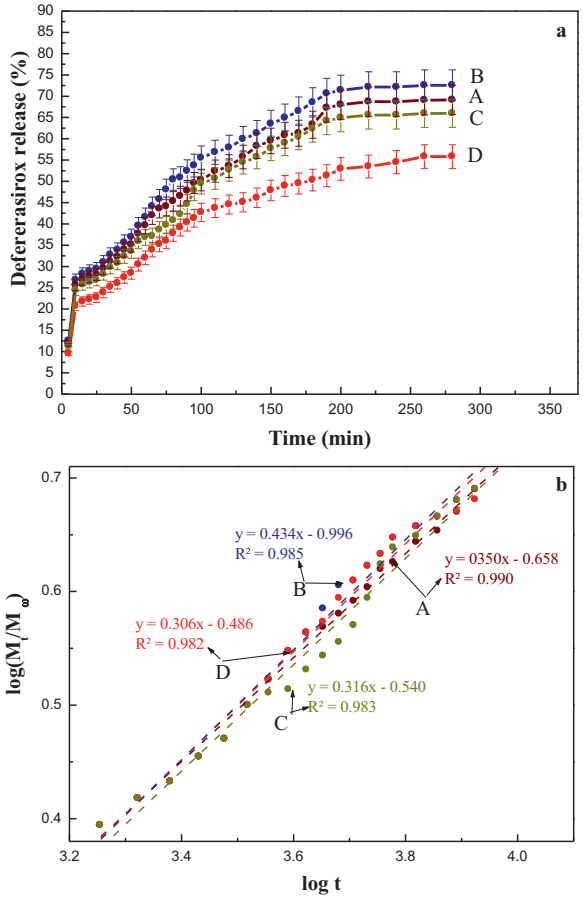

Fig. 8. (a) Effect of loading, and (b) plots of $\log(M_t/M_\infty)$ vs. $\log t$ for deferasirox on its release profiles from loaded hydrogels (samples A–D; 0.05 g) at pH = 7 phosphate buffer.

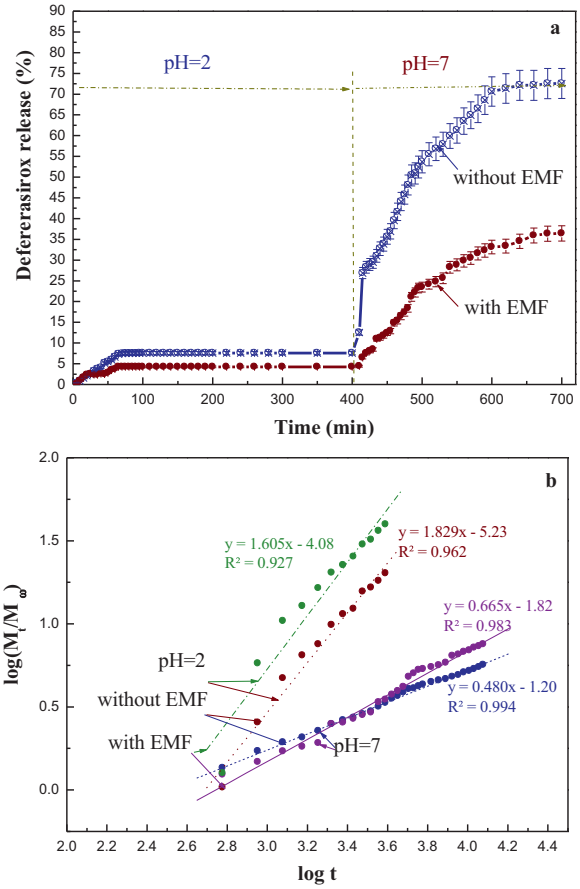

Fig. 9. (a) Deferasirox release from sample B, and (b) plots of $\log(M_t/M_\infty)$ vs. $\log t$ for this sample in different media at 37 °C in the presence and absence of EMF.

followed by sustained release at pH 7 without significant initial burst release. The relatively low amount of deferasirox released from the MION–salep hydrogel at pH 2 solution was probably related to the comparatively low swelling degree of MION–salep hydrogel at pH 2 (Fig. 2d). At pH 7, the amount of deferasirox released increased significantly because the swelling of the hydrogel network increased at neutral pH. This experiment was also done in the presence of EMF and results are shown in Fig. 9a. Compared to former experiment, deferasirox release occurred slightly lower than the release in the absence of EMF. This lower deferasirox release at pH 7 suggests that the EMF has a more marked influence on the release process (Liu et al., 2006). To better investigation of mechanisms in these experiments, Eq. (3) was used. Fig. 9b shows $\log(M_t/M_\infty)$ vs. $\log t$ curves for deferasirox release from MION–salep hydrogel (sample B) in different media at 37 °C in the presence and absence of EMF. Table 2 summarizes data of Fig. 9b. Both values of n for deferasirox at pH 2 are greater than 0.89, indicating that the releases of deferasirox are super case-II transport. For the deferasirox release at pH 7 and in the absence of EMF, the n values are greater than 0.45 and much smaller than 0.89, corresponding to anomalous transport. In this case the polymer relaxation time is comparable to the diffusion time and the release behavior follows both diffusion and polymer relaxation controlled kinetics. For the deferasirox release at pH 7 and in the presence of EMF, the n values are very close to 0.89, which corresponds to anomalous transport. In this case, this n value emphasizes that the deferasirox release tends to be more controlled by polymer relaxation than diffusion. This phenomenon may be attributed to the tendency of magnetic moments of the MION to align with the external magnetic fields for producing a bulk magnetic moment.

Table 2
Release exponent (n), rate constant ($\log k$), and correlation coefficient (R^2) for deferasirox release from MION–salep hydrogel (sample B) at 37 °C in the presence and absence of EMF.

Condition	pH = 2			pH = 7		
	Log k	n	R^2	Log k	n	R^2
Absence of EMF	−5.23	1.829	0.962	−1.20	0.480	0.971
Presence of EMF	−4.08	1.605	0.927	−1.82	0.665	0.983

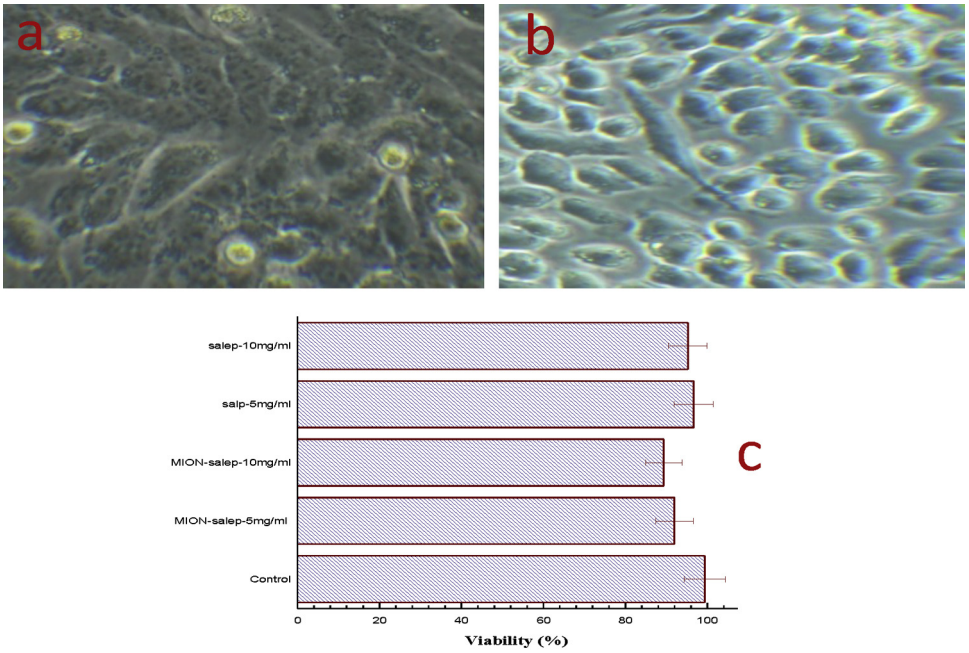

Fig. 10. Inverted microscopic view of cytotoxicity test of (a) HTB 5637 cell line before treatment, (b) after 24 h treatment with MION–salep hydrogel, and (c) cytotoxicity investigation of MION–salep hydrogel on HTB 5637 cells. (For interpretation of the references to color in citation of this figure, the reader is referred to the web version of this article.)

Therefore, MION tempt to aggregate and reduce porosity size of hydrogel which prevent diffusion of deferasirox from MION–salep hydrogel (Liu et al., 2006; Zhou et al., 2012).

3.5. Cell biocompatibility

It is well known that materials with cell viability more than 80% are often recognized as biocompatible (Ying & Hwang, 2010). In our experiment biocompatibility of the MION–salep hydrogel was investigated using MTT assay and the percentage cell viability results are illustrated in Fig. 10. The changes in the color of Fig. 10a–c are attributed to reaction of MION–salep hydrogel and MTT with HTB 5637 cells. As shown in Fig. 10d the viability analysis indicated values of MION–salep hydrogel are 91.28 and 89.64% for 5 and 10 mg/mL, respectively, which are slightly lower than salep. These results confirm that the MION–salep hydrogel exhibits good biocompatibility at high concentration, which are in good agreement with the previous reported results (Mahmoudi et al., 2011). It makes MION–salep hydrogel suitable for biomedical applications.

4. Conclusions

In conclusion, MION–salep hydrogel was successfully prepared by simultaneous formation of MION and salep hydrogel in one-pot method. The structural analysis of the MION–salep hydrogel confirmed the presence of the feed components in the MION–salep hydrogel. Thermal stability of the salep was increased about 34% at 700 °C by increasing the MION in salep which more confirmed the presence of MION in salep hydrogel. The results of VSM exhibited that the MION–salep hydrogel has a superparamagnetic property. The considerable temperature, pH, and EMF sensitivity of MION–salep hydrogel was used for the in vitro release of deferasirox. The MTT assay of MION–salep hydrogel exhibited a reasonable biocompatibility. Based on these experiments, we suggest that the one-pot synthesis of MION/salep hydrogel presented in this paper can represent a new method for constructing magnetic carrier for drug delivery systems and it will enable expanding applications to construct other types of magnetic drug delivery systems in the future.

Acknowledgements

We are grateful to the PNU and INSF for funding this work.

References

Ali, A. E., & AlArifi, A. (2009). Characterization and in vitro evaluation of starch based hydrogels as carriers for colon specific drug delivery systems. *Carbohydrate Polymers*, *78*, 725–730.

Andreas, K., Georgieva, R., Ladwig, M., Mueller, S., Notter, M., Sittinger, M., et al. (2012). Highly efficient magnetic stem cell labeling with citrate-coated superparamagnetic iron oxide nanoparticles for MRI tracking. *Biomaterials*, *33*, 4515–4525.

Angelucci, E., Brittenham, G. M., McLaren, C. E., Ripalti, M., Baronciani, D., Giardini, C., et al. (2000). Hepatic iron concentration and total body iron stores in thalassemia major. *New England Journal of Medicine*, *343*(5), 327–331.

Bardajee, G. R., Hooshyar, Z., & Jafarpour, F. (2013). Antibacterial and optical properties of a new water soluble CdSe quantum dots coated by multidentate biopolymer. *Journal of Photochemistry and Photobiology A: Chemistry*, *252*, 46–52.

Bardajee, G. R., Hooshyar, Z., & Rezanezhad, H. (2012). A novel and green biomaterial based silver nanocomposite hydrogel: Synthesis, characterization and antibacterial effect. *Journal of Inorganic Biochemistry*, *117*, 367–373.

Brittenham, G. M., Allen, C. J., Farrell, D. E., & Harris, J. W. (1989). Hepatic iron stores in thalassemia: Non-invasive magnetic measurements. *Progress in Clinical and Biological Research*, *309*, 101–106.

Brittenham, G. M., Farrell, D. E., Harris, J. W., Feldman, E. S., Danish, E. H., Muir, W. A., et al. (1982). Magnetic-susceptibility measurement of human iron stores. *New England Journal of Medicine*, *307*(27), 1671–1675.

Brunsen, A., Utech, S., Maskos, M., Knoll, W., & Jonas, U. (2012). Magnetic composite thin films of Fe_xO_y nanoparticles and photocrosslinked dextran hydrogels. *Journal of Magnetism and Magnetic Materials*, *324*, 1488–1497.

Calmon, M. F., Souza, A. T., Candido, N. M., Raposo, M. I. B., Taboga, S., Rahal, P., et al. (2012). A systematic study of transfection efficiency and cytotoxicity in HeLa cells using iron oxide nanoparticles prepared with organic and inorganic bases. *Colloids and Surfaces B: Biointerfaces*, *100*, 177–184.

Chung, E., Kim, H., Lee, G., Kwak, B., Jung, J., Kuh, H., et al. (2012). Design of deformable chitosan microspheres loaded with superparamagnetic iron oxide nanoparticles for embolotherapy detectable by magnetic resonance imaging. *Carbohydrate Polymers*, *90*, 1725–1731.

Cole, A. J., David, A. E., Wang, J., Galbán, C. J., Hill, H. L., & Yang, V. C. (2011). Polyethylene glycol modified, cross-linked starch-coated iron oxide nanoparticles for enhanced magnetic tumor targeting. *Biomaterials*, *32*, 2183–2193.

Cole, A. J., David, A. E., Wang, J., Galbán, C. J., & Yang, V. C. (2011). Magnetic brain tumor targeting and biodistribution of long-circulating PEG-modified, cross-linked starch-coated iron oxide nanoparticles. *Biomaterials*, *32*, 6291–6301.

Cursaru, B., Teodorescu, M., Boscornea, C., Stanescu, P. O., & Stoleriu, S. (2013). Drug absorption and release properties of crosslinked hydrogels based on diepoxy-terminated poly(ethylene glycol)s and aliphatic polyamines: A study on the effect of the gel molecular structure. *Materials Science and Engineering: C*, *33*, 1307–1314.

Debrassi, A., Bürger, C., Rodrigues, C. A., Nedelko, N., Ślawska-Waniewska, A., Dłużewski, P., et al. (2011). Synthesis, characterization and in vitro drug release of magnetic N-benzyl-O-carboxymethylchitosan nanoparticles loaded with indomethacin. *Acta Biomaterialia*, *7*, 3078–3085.

Dias, A. M. G. C., Hussain, A., Marcos, A. S., & Roque, A. C. A. (2011). A biotechnological perspective on the application of iron oxide magnetic colloids modified with polysaccharides. *Biotechnology Advances*, *29*, 142–155.

Easo, S. L., & Mohanan, P. V. (2013). Dextran stabilized iron oxide nanoparticles: Synthesis, characterization and in vitro studies. *Carbohydrate Polymers*, *92*, 726–732.

Farhoosh, R., & Riazi, A. (2007). A compositional study on two current types of salep in Iran and their rheological properties as a function of concentration and temperature. *Food Hydrocolloids*, *21*, 660–666.

Figuerola, A., Corato, R. D., Manna, L., & Pellegrino, T. (2010). From iron oxide nanoparticles towards advanced iron-based inorganic materials designed for biomedical applications. *Pharmacological Research*, *62*, 126–143.

Fuhrer, R., Athanassiou, E. K., Luechinger, N. A., & Stark, W. J. (2009). Crosslinking metal nanoparticles into the polymer backbone of hydrogels enables preparation of soft, magnetic field-driven actuators with muscle-like flexibility. *Small*, *5*, 383–388.

Gajendiran, M., Gopi, V., Elangovan, V., Murali, R. V., & Balasubramanian, S. (2013). Isoniazid loaded core shell nanoparticles derived from PLGA–PEG–PLGA triblock copolymers: In vitro and in vivo drug release. *Colloids and Surfaces B: Biointerfaces*, *104*, 107–115.

Gao, S., Guo, J., & Nishinari, K. (2008). Thermoreversible konjac glucomannan gel crosslinked by borax. *Carbohydrate Polymers*, *72*, 315–325.

Goloverda, G., Jackson, B., Kidd, C., & Kolesnichenko, V. (2009). Synthesis of ultrasmall magnetic iron oxide nanoparticles and study of their colloid and surface chemistry. *Journal of Magnetism and Magnetic Materials*, *321*, 1372–1376.

Gordon, T., Perlstein, B., Houbara, O., Felner, I., Banin, E., & Margel, S. (2011). Synthesis and characterization of zinc/iron oxide composite nanoparticles and their antibacterial properties. *Colloids and Surfaces A: Physicochemical and Engineering Aspects*, *374*, 1–8.

Gui, R., Wan, A., Jin, H., Li, H., & Zhou, C. (2013). Amphiphilic polymer-template synthesis and pH-triggered phase transfer of luminescent silver nanocrystals. *Materials Letters*, *96*, 20–23.

Guo, J., Jin, Y., Yang, X., Yu, S., Yin, S., & Qi, J. (2013). Computed microtomography and mechanical property analysis of soy protein porous hydrogel prepared by homogenizing and microbial transglutaminase cross-linking. *Food Hydrocolloids*, *31*, 220–226.

Gupta, N. V., & Shivakumar, H. G. (2010). Preparation and characterization of superporous hydrogels as gastroretentive drug delivery system for rosiglitazone maleate. *DARU*, *18*, 200–210.

Ha, W., Wu, H., Ma, Y., Fan, M., Peng, S., Ding, L., et al. (2013). Synthesis of biocompatible hybrid magnetic hollow spheres based on encapsulation strategy. *Carbohydrate Polymers*, *92*, 523–528.

Ha, W., Wu, H., Wang, X., Peng, S., Ding, L., Zhang, S., et al. (2011). Self-aggregates of cholesterol-modified carboxymethyl konjac glucomannan conjugate: Preparation, characterization, and preliminary assessment as a carrier of etoposide. *Carbohydrate Polymers*, *86*, 513–519.

Hernández, R., & Mijangos, C. (2009). In situ synthesis of magnetic iron oxide nanoparticles in thermally responsive alginate-poly(N-isopropylacrylamide) semi-interpenetrating polymer networks. *Macromolecular Rapid Communications*, *30*, 176–181.

Hezaveh, H., & Muhamad, I. I. (2012). The effect of nanoparticles on gastrointestinal release from modified κ-carrageenan nanocomposite hydrogels. *Carbohydrate Polymers*, *89*, 138–145.

Hozumi, T., Yoshida, M., Ishida, Y., Mimoto, H., Sawa, J., Doi, K., et al. (1995). Long-term effects of dietary fiber supplementation on serum glucose and lipoprotein levels in diabetic rats fed a high cholesterol diet. *Endocrine Journal*, *42*, 187–192.

Jayapaul, J., Hodenius, M., Arns, S., Lederle, W., Lammers, T., Comba, P., et al. (2011). FMN-coated fluorescent iron oxide nanoparticles for RCP-mediated targeting and labeling of metabolically active cancer and endothelial cells. *Biomaterials*, *32*, 5863–5871.

Jain, T. K., Foy, S. P., Erokwu, B., Dimitrijevic, S., Flask, C. A., & Labhasetwar, V. (2009). Magnetic resonance imaging of multifunctional pluronic stabilized iron-oxide nanoparticles in tumor-bearing mice. *Biomaterials*, *30*, 6748–6756.

Jiang, F., Fu, Y., Zhu, Y., Tang, Z., & Sheng, P. (2012). Fabrication of iron oxide/silica core–shell nanoparticles and their magnetic characteristics. *Journal of Alloys and Compounds*, *543*, 43–48.

Jovanović, Z., Radosavljević, A., Kačarević-Popović, Z., Stojkovska, J., Perić-Grujić, A., Ristić, M., et al. (2013). Bioreactor validation and biocompatibility of Ag/poly(N-vinyl-2-pyrrolidone) hydrogel nanocomposites. *Colloids and Surfaces B: Biointerfaces*, *105*, 230–235.

Kaya, S., & Tekin, A. R. (2001). The effect of salep content on the rheological characteristics of a typical ice-cream mix. *Journal of Food Engineering*, *47*, 59–62.

Khan, A., El-Toni, A. M., & Alhoshan, M. (2012). Preparation of thermo-responsive hydrogel-coated magnetic nanoparticles. *Materials Letters*, *89*, 12–15.

Krukemeyer, M. G., Krenn, V., Jakobs, M., & Wagner, W. (2012). Mitoxantrone-iron oxide biodistribution in blood, tumor, spleen, and liver-magnetic nanoparticles in cancer treatment. *Journal of Surgical Research*, *175*, 35–43.

Ktistis, G., & Georgakopoulos, P. P. (1991). Reology of salep mugilages. *Pharmazie*, *46*, 55–56.

Kuckling, D., Harmon, M. E., & Frank, C. W. (2002). Photo-cross-linkable PNIPAAm copolymers. 1. Synthesis and characterization of constrained temperature-responsive hydrogel layers. *Macromolecules*, *35*, 6377–6383.

Lai, B., Yeh, C., & Chen, D. (2012). Surface modification of iron oxide nanoparticles with polyarginine as a highly positively charged magnetic nano-adsorbent for fast and effective recovery of acid proteins. *Process Biochemistry*, *47*, 799–805.

Lee, J., Jung, M. J., Hwang, Y. H., Lee, Y. J., Lee, S., Lee, D. Y., et al. (2012). Heparin-coated superparamagnetic iron oxide for in vivo MR imaging of human MSCs. *Biomaterials*, *33*, 4861–4871.

Liang, Y., Zhang, L., Jiang, W., & Li, W. (2007). Embedding magnetic nanoparticles into polysaccharide-based hydrogels for magnetically assisted bioseparation. *A European Journal of Chemical Physics and Physical Chemistry*, *8*, 2367–2372.

Likhitkar, S., & Bajpai, A. K. (2012). Magnetically controlled release of cisplatin from superparamagnetic starch nanoparticles. *Carbohydrate Polymers*, *87*, 300–308.

Li, Q., Xia, B., Branham, M., Ha, W., Wu, H., Peng, S., et al. (2011). Self-assembly of carboxymethyl konjac glucomannan-*g*-poly(ethylene glycol) and (α-cyclodextrin) to biocompatible hollow nanospheres for glucose oxidase encapsulation. *Carbohydrate Polymers*, *86*, 120–126.

Liu, T., Hu, S., Liu, T., Liu, D., & Chen, S. (2006). Magnetic-sensitive behavior of intelligent ferrogels for controlled release of drug. *Langmuir*, *22*, 5974–5978.

Luo, Y., Teng, Z., Wang, X., & Wang, Q. (2013). Development of carboxymethyl chitosan hydrogel beads in alcohol-aqueous binary solvent for nutrient delivery applications. *Food Hydrocolloids*, *31*, 332–339.

Mahmoudi, M., Sant, S., Wang, B., Laurent, S., & Sen, T. (2011). Superparamagnetic iron oxide nanoparticles (SPIONs): Development, surface modification and applications in chemotherapy. *Advanced Drug Delivery Reviews*, *63*, 24–46.

Marzio, L., Bianco, R. D., Donne, M., Pieramico, O., & Cuccurullo, F. (1989). Mouth-to-cecum transit time in patients affected by chronic constipation: Effect of glucomannan. *American Journal of Gastroenterology*, *84*, 888–891.

Matalanis, A., & McClements, D. J. (2013). Hydrogel microspheres for encapsulation of lipophilic components: Optimization of fabrication and performance. *Food Hydrocolloids*, *31*, 15–25.

Monson, T. C., Venturini, E. L., Petkov, V., Ren, Y., Lavin, J. M., & Huber, D. L. (2013). Large enhancements of magnetic anisotropy in oxide-free iron nanoparticles. *Journal of Magnetism and Magnetic Materials*, *331*, 156–161.

Nishioa, Y., Yamadab, A., Ezakib, K., Miyashitab, Y., Furukawab, H., & Horie, K. (2004). Preparation and magnetometric characterization of iron oxide-containing alginate/poly(vinyl alcohol) networks. *Polymer*, *45*, 7129–7136.

Palmer, D., Levina, M., Douroumis, D., Maniruzzaman, M., Morgan, D. J., Farrell, T. P., et al. (2013). Mechanism of synergistic interactions and its influence on drug release from extended release matrices manufactured using binary mixtures of polyethylene oxide and sodium carboxymethylcellulose. *Colloids and Surfaces B: Biointerfaces*, *104*, 174–180.

Paques, J. P., Linden, E., Rijn, C. J. M., & Sagis, L. M. C. (2013). Alginate submicron beads prepared through w/o emulsification and gelation with $CaCl_2$ nanoparticles. *Food Hydrocolloids*, *31*, 428–434.

Parham, H., Zargar, B., & Rezazadeh, M. (2012). Removal, preconcentration and spectrophotometric determination of picric acid in water samples using modified magnetic iron oxide nanoparticles as an efficient adsorbent. *Materials Science and Engineering: C*, *32*, 2109–2114.

Parham, H., Zargar, B., & Shiralipour, R. (2012). Fast and efficient removal of mercury from water samples using magnetic iron oxide nanoparticles modified with 2-mercaptobenzothiazole. *Journal of Hazardous Materials*, *205-206*, 94–100.

Perez-Moral, N., & Gonzalez, M. C. (2013). Preparation of iron-loaded alginate gel beads and their release characteristics under simulated gastrointestinal conditions. *Food Hydrocolloids*, *31*, 114–120.

Pichayakorn, W., & Boonme, P. (2013). Evaluation of cross-linked chitosan microparticles containing metronidazole for periodontitis treatment. *Materials Science and Engineering: C*, *33*, 1197–1202.

Pourjavadi, A., Doulabi, M., Soleyman, R., Sharif, S., & Eghtesadi, S. A. (2012). Synthesis and characterization of a novel (salep phosphate)-based hydrogel as a carrier matrix for fertilizer release. *Reactive and Functional Polymers*, *72*, 667–672.

Pourjavadi, A., Hosseini, S. H., & Fakoorpoor, S. M. (2013). Ionic modified crosslinked salep: A highly loaded and efficient heterogeneous organocatalyst. *Carbohydrate Polymers*, *92*, 2252–2256.

Qin, C., Li, C., Hu, Y., Shen, J., & Ye, M. (2009). Facile synthesis of magnetic iron oxide nanoparticles using 1-methyl-2-pyrrolidone as a functional solvent. *Colloids and Surfaces A: Physicochemical and Engineering Aspects*, *336*, 130–134.

Reddy, N. N., Varaprasad, K., Ravindra, S., Reddy, G. V. S., Reddy, K. M. S., Reddy, K. M. M., et al. (2011). Evaluation of blood compatibility and drug release studies of gelatin based magnetic hydrogel nanocomposites. *Colloids and Surfaces A: Physicochemical and Engineering Aspects*, *385*, 20–27.

Reffo, G. C., Ghirardi, P. E., & Forattani, C. (1990). Double-blind evaluation of glucomannan versus placebo in postinfarcted patients after cardiac rehabilitation. *Current Therapeutic Research*, *47*, 753–758.

Roque, A. C. A., Bicho, A., Batalha, I. L., Cardoso, A. S., & Hussain, A. (2009). Biocompatible and bioactive gum Arabic coated iron oxide magnetic nanoparticles. *Journal of Biotechnology*, *144*, 313–320.

Rubio-Retama, J., Zafeiropoulos, N. E., Serafinelli, C., Rojas-Reyna, R., Voit, B., Cabarcos, E. L., et al. (2007). Synthesis and characterization of thermosensitive PNIPAM microgels covered with superparamagnetic γ-Fe_2O_3 nanoparticles. *Langmuir*, *23*, 10280–10285.

Saeidian, H., Moghaddam, F. M., Pourjavadi, A., Barzegar, S., Soleyman, R., & Sohrabi, A. (2009). Superabsorbent polymer as nanoreactors for preparation of hematite nanoparticles and application of the prepared nanocatalyst for the Friedel–Crafts acylation. *Journal of the Brazilian Chemical Society*, *20*, 466–471.

Schweiger, C., Pietzonka, C., Heverhagen, J., & Kissel, T. (2011). Novel magnetic iron oxide nanoparticles coated with poly(ethylene imine)-g-poly(ethylene glycol) for potential biomedical application: Synthesis, stability, cytotoxicity and MR imaging. *International Journal of Pharmaceutics*, *408*, 130–137.

Shen, C., Juang, J., Tsai, Z., Wu, S., Tsai, F., Wang, J., et al. (2011). Preparation, characterization and application of superparamagnetic iron oxide encapsulated with N-[(2-hydroxy-3-trimethylammonium)propyl] chitosan chloride. *Carbohydrate Polymers*, *84*, 781–787.

Shen, Z., Duan, H., & Frey, H. (2007). Water-soluble fluorescent Ag nanoclusters obtained from multiarm star poly(acrylic acid) as "molecular hydrogel" templates. *Advanced Materials*, *19*, 349–352.

Shirsath, S. R., Patil, A. P., Patil, R., Naik, J. B., Gogate, P. R., & Sonawane, S. H. (2013). Removal of brilliant green from wastewater using conventional and ultrasonically prepared poly(acrylic acid) hydrogel loaded with kaolin clay: A comparative study. *Ultrasonics Sonochemistry*, *20*, 914–923.

Tang, Q., Huang, K., Qian, G., & Benicewicz, B. C. (2013). Phosphoric acid-imbibed three-dimensional polyacrylamide/poly(vinyl alcohol) hydrogel as a new class of high-temperature proton exchange membrane. *Journal of Power Sources*, *229*, 36–41.

Vuksan, V., Jenkins, D. J., Spadafora, P., Sievenpiper, J. L., Owen, R., & Vidgen, E. (1999). Konjac-mannan (glucomannan) improves glycemia and other associated risk factors for coronary heart disease in type 2 diabetes. *Diabetes Care*, *22*, 913–919.

Vu-Quang, H., Muthiah, M., Kim, Y., Cho, C., Namgung, R., Kim, W. J., et al. (2012). Carboxylic mannan-coated iron oxide nanoparticles targeted to immune cells for lymph node-specific MRI in vivo. *Carbohydrate Polymers*, *88*, 780–788.

Vu-Quang, H., Yoo, M., Jeong, H., Lee, H., Muthiah, M., Rhee, J. H., et al. (2011). Targeted delivery of mannan-coated superparamagnetic iron oxide nanoparticles to antigen-presenting cells for magnetic resonance-based diagnosis of metastatic lymph nodes in vivo. *Acta Biomaterialia*, *7*, 3935–3945.

Xu, H., Aguilar, Z. P., Yang, L., Kuang, M., Duan, H., Xiong, Y., et al. (2011). Antibody conjugated magnetic iron oxide nanoparticles for cancer cell separation in fresh whole blood. *Biomaterials*, *32*, 9758–9765.

Ying, E., & Hwang, H. (2010). In vitro evaluation of the cytotoxicity of iron oxide nanoparticles with different coatings and different sizes in A3 human T lymphocytes. *Science of the Total Environment*, *408*, 4475–4481.

Yu, S., Hsieh, H., Pang, J., Tang, D., Shih, C., Tsai, M., et al. (2013). Active films from water-soluble chitosan/cellulose composites incorporating releasable caffeic acid for inhibition of lipid oxidation in fish oil emulsions. *Food Hydrocolloids*, *32*, 9–19.

Yu, S., Wu, G., Gu, X., Wang, J., Wang, Y., Gao, H., et al. (2013). Magnetic and pH-sensitive nanoparticles for antitumor drug delivery. *Colloids and Surfaces B: Biointerfaces*, *103*, 15–22.

Walsh, D. E., Yaghoubian, V., & Behforooz, A. (1984). Effect of glucomannan on obese patients – A clinical study. *International Journal of Obesity*, *8*, 289–295.

Wang, B., Liao, L., Huang, Q., & Cheng, Y. (2011). Adsorption behaviors of benzonic acid by carboxyl methyl konjac glucomannan gel micropheres cross-linked with Fe^{3+}. *Journal of Chemical and Engineering Data*, *57*(1), 72–77.

Wang, R., Xia, B., Li, B., Peng, S., Ding, L., & Zhang, S. (2008). Semi-permeable nanocapsules of konjac glucomannan–chitosan for enzyme immobilization. *International Journal of Pharmaceutics*, *364*, 102–107.

Zhou, L., He, B., & Zhang, F. (2012). Facile one-pot synthesis of iron oxide nanoparticles cross-linked magnetic poly(vinyl alcohol) gel beads for drug delivery. *ACS Applied Materials and Interfaces*, *4*, 192–199.